RSC Advances

PAPER

View Article Online
View Journal | View Issue

Cite this: *RSC Adv.*, 2015, **5**, 75746

Highly efficient colorimetric detection of ATP utilizing a split aptamer target binding strategy and superior catalytic activity of graphene oxide–platinum/gold nanoparticles†

Siqi Zhang,[a] Kun Wang,[ab] Jiali Li,[a] Zhenyu Li[a] and Ting Sun*[a]

In this study, a highly efficient colorimetric assay for adenosine triphosphate (ATP) was constructed based on a split aptamer target binding strategy and grapheme oxide–platinum/gold nanoparticle platform to increase catalytic properties. Platinum/gold nanoparticles were easily prepared by reducing the mixture solution of K_2PtCl_6 and $HAuCl_4$ using sodium citrate in a one-pot synthesis. Next, graphene oxide/platinum/gold nanoparticle hybrids (GO/PDDA/$PtAu_{NPs}$) were fabricated using a self-assembly procedure. Ultrasensitive and enzyme-free detection of ATP in fetal bovine serum was achieved using split aptamer-modified magnetic beads as a separating unit and split aptamer-modified GO/PDDA/$PtAu_{NPs}$ as a catalyst-detecting platform. The specific binding of ATP and its aptamer linked the split aptamer-modified GO/PDDA/$PtAu_{NPs}$ and magnetic beads together. Using magnetic separation, achromatous tetramethylbenzidine was catalyzed into a colored product by separated nanocomposites, which enabled rapid detection of ATP. The color change caused by the low concentration ATP (50 nM) was clearly distinguished by direct observation. The detection limit of the colorimetric assay for ATP was 0.2 nM, which is close to the lowest detection limit for colorimetric detection of ATP. This assay showed excellent selectivity against guanosine triphosphate, uridine triphosphate, and cytosine triphosphate and can be applied in real samples.

Received 10th July 2015
Accepted 28th August 2015

DOI: 10.1039/c5ra13550h

www.rsc.org/advances

1. Introduction

Graphene, a single-atom-thick 2D nanomaterial, has gained attention in materials science and biotechnology because of its advantageous electronic, thermal, and mechanical properties.[1,2] Graphene oxide (GO) is an oxidized derivative of graphene with excellent water solubility, and it has been used to design new types of biosensors and diagnostic platforms.[3] Recently, Qu *et al.*[1] reported that graphene oxide has intrinsic peroxidase-like activity, which can catalyze the reaction of the peroxidase substrate 3,3,5,5-tetramethylbenzidine (TMB) in the presence of H_2O_2 to produce a blue color. The extremely large surface area of graphene oxide also provides a good platform for assembling various highly efficient peroxidase-like nanomaterials, such as platinum/gold nanoparticle hybrids.[4] Compared with natural horseradish peroxidase,[5] which is more expensive and difficult to prepare and purify,[6] graphene oxide/platinum/gold nanoparticle hybrids (GO/$PtAu_{NPs}$) are more stable in analytical processes and shows better catalytic activity.

Currently, nanomaterials have attracted attention in different fields because of their unique size and electronic, optical, catalytic properties.[7,8] The appropriate linkage of different types of nanostructured materials can be used exploited to prepare various types of nanosensors. For instance, small molecule-triggered linkage of split aptamer fragments has been widely applied in nanoanalysis.[9] Single-strand DNA aptamers are chemical synthetic oligonucleotides acquired from a selective process known as SELEX. The aptamers and target can form a complex that shows excellent selectivity and stability.[10] For example, the 27-base ATP aptamer was divided into two different sequences. The two split aptamers did not interact in the absence of ATP.[9,11] ATP serves as the major "energy currency" in most organisms and therefore plays an important role in many cellular processes.[12] ATP transports chemical energy within cells for metabolism. Since ATP can support living activities in biological tissues, measuring its concentration is very important in the biochemical field. Numerous methods have been developed to detect ATP, such as electrochemical luminescence,[13–16] chemiluminescence,[17] liquid chromatography,[18,19] electrical analysis,[20–22] fluorescence spectrophotometry,[23–25] and fluorescence resonance energy

[a]*College of Sciences, Northeastern University, Shenyang, 110819, China. E-mail: sun1th@163.com; Tel: +86-024-83684786*

[b]*Department of Chemistry and Environmental Engineering, Changchun University of Science and Technology, Changchun, China*

† Electronic supplementary information (ESI) available. See DOI: 10.1039/c5ra13550h

transfer.[26] However, these detection methods have inherent drawbacks such as high-cost, time-consuming processes, and expensive instruments. Thus, it is necessary to develop an ultrasensitive method for detecting ATP that is simpler and more selective.

Nanomaterial-based colorimetric assays are simple, low cost, label-free, and show convenient readouts for non-instrument detection.[27–29] Gold nanoparticles[30,31] have been used in colorimetric assays because of their size-dependent surface plasmon resonance adsorption properties; these nanoparticles were first used to detect ATP in 2007.[32] However, gold nanoparticles are not stable and are readily aggregated in solutions with high salt concentrations, limiting their applicability in research.[33] Thus, signal amplification strategies have been developed to increase detective sensitivity.[34] ATP split-aptamer fragments were utilized to link the functionalized graphene and magnetic beads in the presence of ATP.[9]

In this study, we developed an ultrasensitive, enzyme free, novel, and visual ATP assay method based on the coupling of the high catalytic activity of GO/$PtAu_{NPs}$ with magnetic beads to achieve specific linkage of split aptamers to targets. Since platinum/gold nanoparticle hybrids and GO have a synergistic effect with enhanced catalytic activity in the TMB–H_2O_2 reaction, ultrasensitive ATP detection can be achieved.

2. Experimental

2.1 Chemicals and materials

Ultrapage-purified oligonucleotides were synthesized by Sangon Biotechnology Co., Ltd. (Shanghai, China). ATP, guanosine triphosphate (GTP), cytidine triphosphate (CTP), uridine triphosphate (UTP), (3-aminopropyl) triethoxysilane, 2-[*N*-morpholino] ethanesulfonic acid (MES), sodium acrylate, and 3,3′,5,5′-tetramethylbenzidine (TMB) were purchased from Sigma-Aldrich (St. Louis, MO, USA). Dimethyl sulfoxide, Tris, potassium chloroplatinate (K_2PtCl_6), and chloroauric acid ($HAuCl_4 \cdot 4H_2O$) were purchased from Aladdin Reagents (Shanghai, China). 1-Ethyl-3-(3-dimethylaminopropyl) carbodiimide hydrochloride and *N*-hydroxysuccinimide were purchased from J&K Chemical (Beijing, China). Potassium chloride, magnesium chloride, potassium acetate, hydrogen peroxide (H_2O_2), ferric chloride, Tween 20, and ethylene glycol were purchased from Beijing Chemical Reagent Company (Beijing, China).

2.2 Instruments

A Cary 60 UV/Vis Spectrophotometer (Agilent Technologies, Santa Clara, CA, USA) was used to quantify the oligonucleotides. Transmission electron microscopy (TEM) measurements were conducted on a Tecnai G2 F20 S-TWIN (FEI, Hillsboro, OR, USA) with an accelerating voltage of 200 kV. Scanning electron microscopy (SEM) measurements were conducted on an ESEMXL-30 (FEI). X-ray photoelectron spectroscopy (XPS) data were acquired using an ESCALab250i-XL electron spectrometer from VG Scientific (Waltham, MA, USA) using 300 W Al Kα radiations.

2.3 Sequences and pretreatment of oligonucleotides

Oligonucleotide sequences were as follows: aptamer-1 (Apt-1): 5′-HOOC-ACCTGGGGGATAAT-3′, aptamer-2 (Apt-2): 5′-TGCGGAGGAAGG TAAAAAAAAAA-SH-3′. Oligonucleotides were stored at −20 °C and were heated to 95 °C for 5 min and gradually cooled to room temperature before use.

2.4 Preparation of aptamer-modified nanoparticles

The detailed procedure of Fe_3O_4@SiO_2 and GO/$PtAu_{NPs}$ preparation and functionalization is described in the ESI.†

2.5 Colorimetric detection

First, 30 μL of Fe_3O_4@SiO_2/aptamer-1 and 30 μL GO/$PtAu_{NPs}$/aptamer-2 were added to 940 μL of Tris–HCl buffer containing ATP and incubated 1 h. After magnetic separation, the sandwich structure of (Fe_3O_4@SiO_2)/aptamer–ATP complex/(GO/$PtAu_{NPs}$) was dispersed into 500 μL of MES–Ac buffer (25 mM MES–Ac, pH 4.5, 20 mM KAc). Next, 25 μL of 15 mM TMB solution and 5 μL of H_2O_2 (30% w/v) were rapidly added to initiate the TMB–H_2O_2 reaction. This reaction was allowed to proceed for 10 min at 25 °C. After the solution had turned blue, the reaction was immediately stopped by separating the nanomaterials and transferring the supernatant solution to another centrifuge tube. A photograph of the reaction product was taken using a digital camera. All photographs were used without further modification.

3. Results and discussion

3.1 Principle of the colorimetric strategy for ATP detection

The principle of the colorimetric biosensor is depicted in Scheme 1. The colorimetric ATP assay is based on the color change of TMB in the presence of H_2O_2.[35–37] According to previous studies,[1,4] PtAu nanoparticles and graphene oxide exhibit peroxidase-like catalytic activity and can catalyze the colorless substrate TMB into a blue color product with the help of H_2O_2. The detection principle is based on a sandwich-type construction that is formed between split-aptamer-modified graphene oxide/$PtAu_{NPs}$ and magnetic beads in the presence of ATP. The aptamer-2 modified on graphene oxide/$PtAu_{NPs}$ and aptamer-1 modified on magnetic beads specifically recognized ATP and these particles were linked together.[38] With the aid of a magnetic field, the complexes were separated and the reaction of peroxidase substrate TMB was catalyzed in the presence of H_2O_2 to produce a blue color solution. In the absence of ATP, split-aptamer fragments did not link together and a signal was not generated. The color change depended on the amount of ATP and was quantitated using a spectrophotometer and by direct observation. Moreover, our approach first utilized graphene oxide/$PtAu_{NPs}$ as an efficient catalyst to achieve ultrasensitive detection of ATP because each aptamer–ATP complex could link hundreds of platinum/gold nanoparticles. The multiple signal amplification strategy increased the sensitivity of the colorimetric assay.

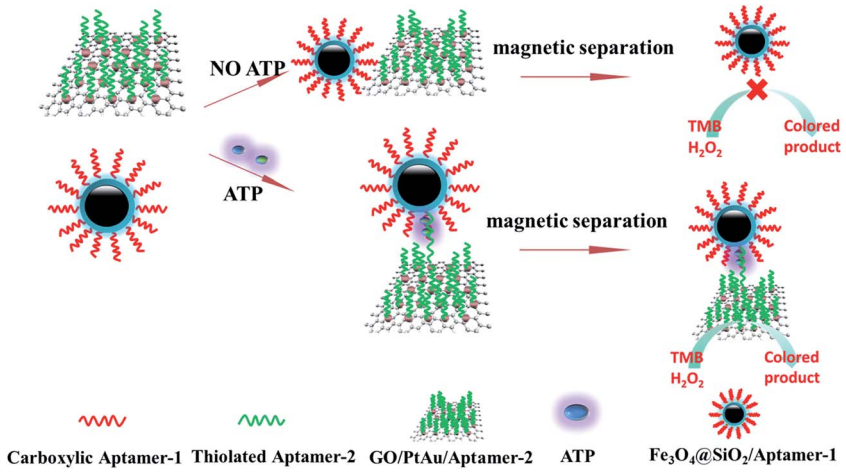

Scheme 1 Schematic illustration of colorimetric detection of ATP on the basis of split aptamer target binding and GO/$PtAu_{NPs}$ catalytic platform.

3.2 Preparation and characterization of the magnetic Fe_3O_4@SiO_2 composites

Magnetic Fe_3O_4@SiO_2 nanoparticles of various sizes have been prepared successfully using several methods. The TEM results (Fig. 1A) showed that the magnetic beads had an average diameter of approximately 200 nm. Through the hydrolysis and condensation of TEOS in the ethanol–ammonia mixture, the silica layer was gradually immobilized onto the surface of Fe_3O_4 nanoparticles. The core–shell structure of Fe_3O_4@SiO_2 nanoparticles is clearly shown in Fig. 1B.

3.3 Optimization of catalyst activity of grapheme oxide–platinum/gold nanoparticles

The loading of the platinum/gold nanoparticles onto GO was characterized by SEM and TEM. Representative images of grapheme oxide–platinum/gold nanoparticles are shown in Fig. 2A and B, respectively. GO was modified by the platinum/gold nanoparticle hybrids, with a large number of $PtAu_{NPs}$ on a single GO. Since bimetallic $PtAu_{NPs}$ exhibit considerable peroxidase-like activity in catalyzing fluorogenic substrates,[4] composite nanomaterials known as GO@$PtAu_{NPs}$ were utilized to catalyze its colorless substrate TMB into a blue color product in the presence of H_2O_2. The catalytic activity of the nanomaterials was investigated by varying the $[Au^{3+}]/[Pt^{4+}]$ molar ratio from 10/0 to 7.0/3.0. As shown in Fig. 3C, GO@Au_{NPs} exhibits the lowest catalytic activity. The catalytic activity gradually increased with an increasing ratio of Pt/Au from GO@Pt_0Au to GO@$Pt_{0.1}$-Au. By further increasing the ratio of Pt/Au, the catalytic activity of GO@PtAu sharply decreased because of the decreasing number of active sites on the surface of the composite nanomaterials. Thus, GO@$Pt_{0.1}Au$ was considered a reasonable catalyst. XPS is used to analyze the surface chemistry of composite nanomaterials (GO@$Pt_{0.1}Au$). The featured peaks in Fig. 3A and B are attributed to Au ($4f_{7/2}$ at 83.4 eV; Au $4f_{5/2}$ at 87 eV), Pt ($4f_{7/2}$ at 70.4 eV; $4f_{5/2}$ at 74.3 eV), and C (1s at 284.78 eV).

3.4 Optimization of other experimental conditions

The optimal assembly time in the self-assembly of nanomaterials was investigated by monitoring the color change of the TMB–H_2O_2 reaction (Fig. 4A). The absorbance value of TMB at 652 nm gradually increased with increasing assembly time to 60 min. Further increasing the assembly time did not result in increased absorbance. Thus, 60 min was used as the assembly time.

As shown in Fig. 4B, the effect of pH values (range: 5–10) on absorbance was also investigated. The absorbance showed no obvious undulation at different pH values. In order to simplify the working processes, a pH of 8 was selected. Fig. 4C shows that increasing the temperature slowly increased the rate of aptamer and target self-assembly. For the convenience of experimental operation, room temperature (25 °C) was chosen as the reaction temperature.

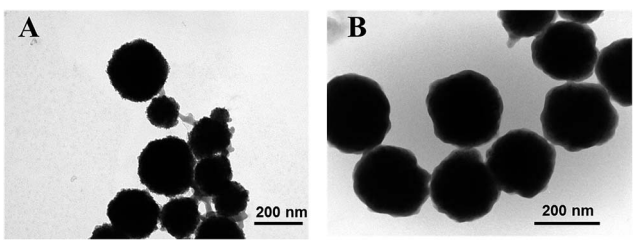

Fig. 1 TEM images of (A) Fe_3O_4 microspheres, (B) magnetic Fe_3O_4@SiO_2 core/shell composites.

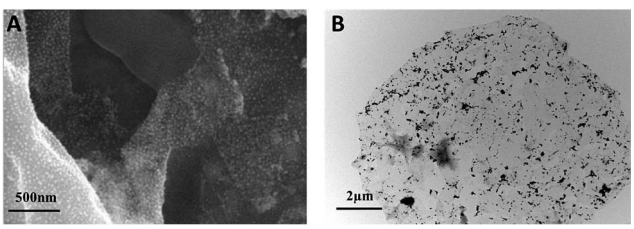

Fig. 2 (A) SEM of the as-prepared GO@$Pt_{0.1}Au$, (B) TEM of the as-prepared GO@$Pt_{0.1}Au$.

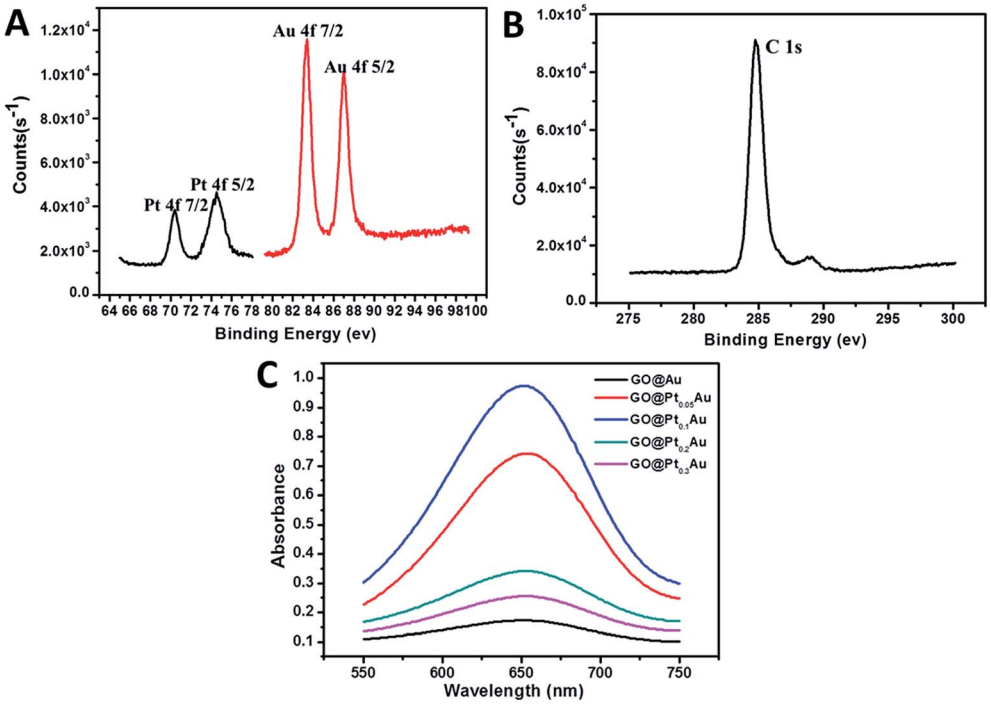

Fig. 3 (A) XPS of Au (red curve) and Pt (black curve) obtained from the as-prepared GO@$Pt_{0.1}$Au, (B) XPS of C (black curve) obtained from the as-prepared GO@$Pt_{0.1}$Au, (C) peroxidase-like activity of GO@PtAu with different ratios of Pt to Au in the colorimetric reaction of TMB in the presence of H_2O_2.

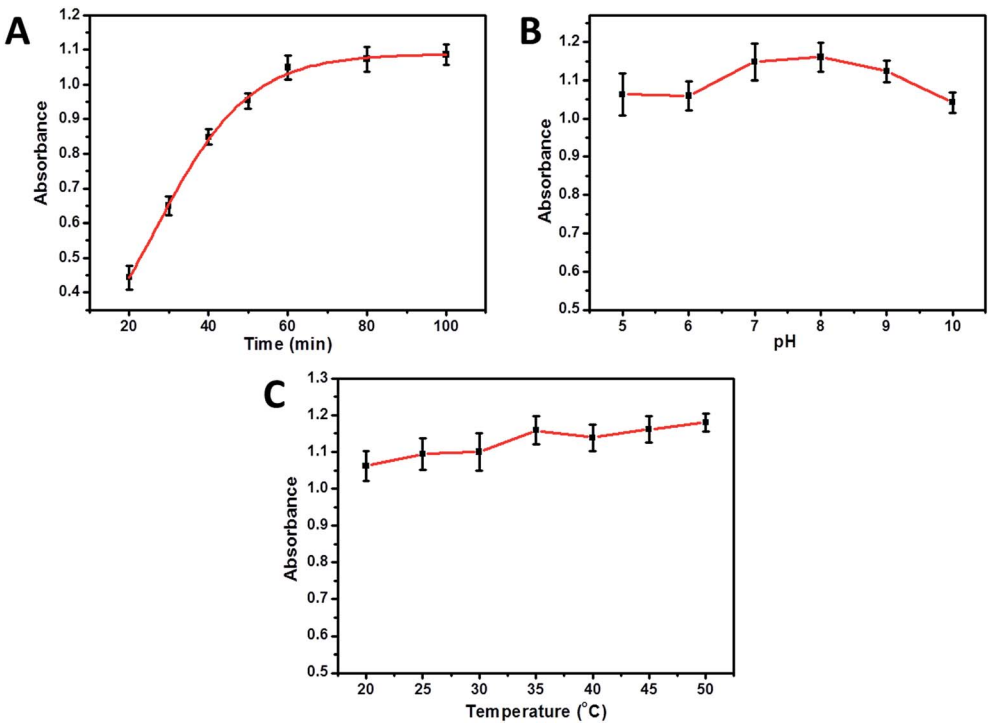

Fig. 4 Effect of (A) assembly time, (B) pH, and (C) temperature during self-assembly of nanomaterial on the absorbance value at 652 nm in presence of 100 nM ATP.

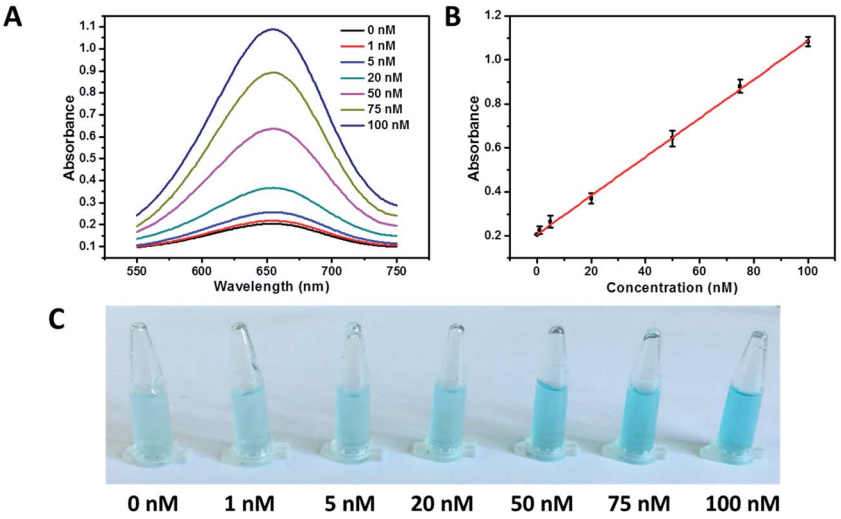

Fig. 5 Sensitivity for ATP detection. (A) UV-vis absorption spectra of the supernatant solution for TMB–H_2O_2 reaction against various concentrations of ATP ranging from 0–100 nM. (B) Linear curve of absorbance value at 652 nm *versus* the ATP concentration. (C) Photo images of the color intensity with various concentrations of ATP (0, 1, 5, 20, 50, 75, and 100 nM).

3.5 Quantitative detection of ATP

The sensitivity of and linear range of the colorimetric method was investigated by monitoring the color and absorbance change in the presence of various concentrations of ATP (0, 1, 5, 20, 50, 75, and 100 nM). In the absence of ATP, the aptamer-2 modified graphene oxide/$PtAu_{NPs}$ did not link with aptamer-1 modified on magnetic beads, but these particles were eliminated through magnetic separation. In the presence of ATP, a sandwich-type construction GO/$PtAu_{NPs}$/aptamer–ATP complex/Fe_3O_4@SiO_2 was gradually generated with increasing concentrations of ATP from 0–100 nM (Fig. 5A), resulting in the color change of the TMB–H_2O_2 system through magnetic separation and re-dispersion (Fig. 5C). As shown in Fig. 5B, the absorbance at 652 nm showed a linear relationship with the concentration of ATP ranging from 0–100 nM. The linear regression equation used was as follows: Abs = 0.206 + 0.0088C_{ATP} (R^2 = 0.999). Error was calculated from three sets of experimental measurement data. Thus, the limit of detection (LOD) of 0.2 nM was calculated according to the equation LOD = 3σ/slope, which is superior to many existing colorimetric sensors (Table 1). The lowest detection limit for colorimetric detection of ATP is 0.2 nM. The detection method is sensitive because of the synergistic action of the high catalytic activity of graphene oxide/platinum/gold nanoparticle hybrids and the magnetic separation technique. Furthermore, it is convenient to distinguish the color of the solution containing 50 nM ATP from the solution without ATP by direct observation (Fig. 4C). Thus, the LOD for visual detection was set to 50 nM.

3.6 Specificity and reproducibility of the colorimetric sensor

The selectivity tests for the colorimetric assay were conducted by examining the absorbance change of the solution containing ATP with that containing the analogs of ATP such as GTP, UTP, and CTP (Fig. 6). A concentration of 100 nM ATP and its analogs was chosen. The strategy showed an excellent specific response against ATP analogs, which was because of the specific recognition between the ATP split aptamer and ATP. The different colorimetric results revealed that the analogs of ATP could not link the magnetic beads and GO/$PtAu_{NPs}$ together, resulting in no obvious color change. Therefore, the nanomaterial-based colorimetric assay can be applied for highly sensitive detection of ATP with high specificity. The reproducibility of the colorimetric aptasensor was evaluated by conducting nine experimental measurements with 100 nM ATP. The aptasensors exhibited similar absorbance intensities (Fig. 7) with a relative standard deviation (RSD) of 5.12%.

Table 1 Detection limits of various methods for ATP colorimetric assay

Analytical method	Detection limit	Reference
Colorimetric detection based on functionalized gold nanoparticles with split aptamer	24 μM	31
Colorimetric detection based on target recycling amplification	0.33 nM	39
Colorimetric detection based on a polythiophene derivative	10 nM	40
Colorimetric detection based on cyclic enzymatic signal amplification and hairpin aptamer probe	25 nM	41
Colorimetric detection based on binding-induced collapse of DNA nano-assembly with plasmonic gold nanoparticles	5 μM	30
Colorimetric detection with DNAzyme	67 nM	42
Colorimetric detection based on split aptamer and catalytic activity of graphene oxide–platinum/gold nanoparticles	0.2 nM	This work

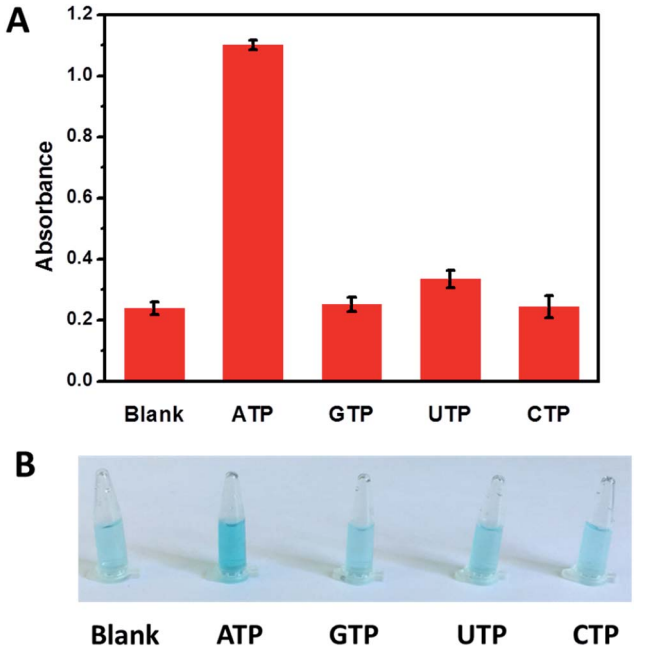

Fig. 6 Selectivity for ATP detection. (A) Histogram of absorbance value at 652 nm of the supernatant solution for TMB–H_2O_2 reaction in the presence of ATP (100 nM), GTP (100 nM), UTP (100 nM), and CTP (100 nM). (B) Photo images of the solution color changed with the ATP and ATP analogs.

3.7 Analysis of ATP in real sample

The ATP assay was conducted using fetal bovine serum to demonstrate the applicability of the colorimetric sensor to laboratory samples. As shown in Fig. 8, the sensor performed well when challenged in 1% fetal bovine serum. The fetal bovine serum had little effect on the analysis, which may have resulted from nonspecific interference. Nevertheless, if 100 nM ATP was present in the pure aqueous buffer or buffer containing 1% fetal bovine serum, an approximately 300% increase in the absorbance value at 652 nm was observed. In order to verify the performance of the method for detecting ATP, the recovery rate for the spiked ATP was determined (Table 2). Compared with other standard methods, the recovery rate of our approach was similar to those of other methods. These results reveal that our nanomaterials can be used to detect ATP in real samples in a sensitive and specific manner using the magnetic separation technique.

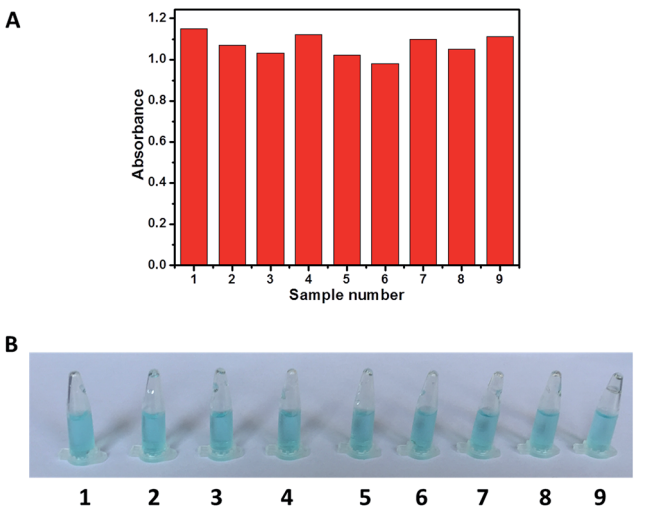

Fig. 7 (A) Histogram of absorbance value at 652 nm for the nine experimental measurements with 100 nM ATP. (B) Photo images of the solution color in the nine experimental measurements.

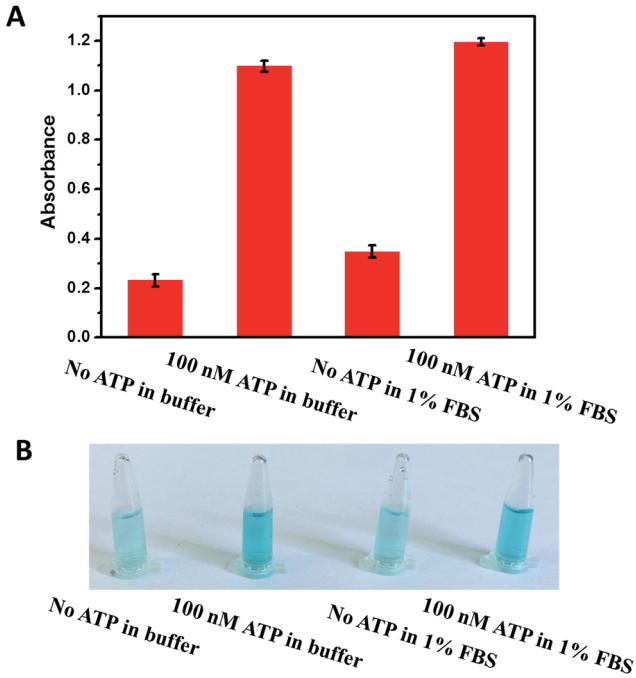

Fig. 8 Determination of ATP in 1% fetal bovine serum. (A) Histogram of absorbance value at 652 nm of the supernatant solution for TMB–H_2O_2 reaction in the presence of 0 nM ATP in buffer, 100 nM ATP in buffer, 0 nM ATP in buffer containing 1% FBS, and 100 nM ATP in buffer containing 1% FBS. (B) Photo images of the solution color in the presence of different matrices.

Table 2 Recovery rate of various methods for ATP sensing

Sensing method	Recovery (%)	Reference
Fluorescence sensor	95.5–102.2	23
SERS sensor	95.1	43
Chemiluminescent sensor	104.7	15
Electrochemical sensor	107	44
Colorimetric sensor	96.3	This work

4. Conclusions

In summary, an ultrasensitive, simple, enzyme-free, and visual ATP biosensor based on the sandwich structure of nanomaterials was developed. The key point of this strategy lies in that ATP can assist in ATP-triggered linkage of split-aptamer fragments between GO/$PtAu_{NPs}$ and Fe_3O_4@SiO_2. By

monitoring the color change after adding TMB and H_2O_2, we detected ATP concentrations as low as 0.2 nM, which is superior over many reported visual sensors for ATP detection. This method can be expanded to analyze other targets because the ATP split aptamer can be altered into other aptamers such as thrombin and kanamycin aptamers in future studies.

Acknowledgements

The project was partly sponsored by the Fundamental Research Funds for the Central Universities of China (grant no. N130605001) and the National Natural Science Foundation of China (No. 21477082).

References

1 Y. J. Song, K. G. Qu, C. Zhao, J. S. Ren and X. G. Qu, *Adv. Mater.*, 2010, **22**, 2206–2210.
2 C. S. Shan, H. F. Yang, J. F. Song, D. X. Han, A. Ivaska and L. Niu, *Anal. Chem.*, 2009, **81**, 2378–2382.
3 J. H. Jung, D. S. Cheon, F. Liu, K. B. Lee and T. S. Seo, *Angew. Chem., Int. Ed.*, 2010, **49**, 5708–5711.
4 C.-W. Tseng, H.-Y. Chang, J.-Y. Chang and C.-C. Huang, *Nanoscale*, 2012, **4**, 6823–6830.
5 U. Khan and J. A. Nicell, *J. Chem. Technol. Biotechnol.*, 2007, **82**, 818–830.
6 L. Han, C. Li, T. Zhang, Q. Lang and A. Liu, *ACS Appl. Mater. Interfaces*, 2015, **7**, 14463–14470.
7 S. Zhang, T. Sun and J. Wang, *Microchim. Acta*, 2015, **182**, 1387–1393.
8 S. Zhang, T. Sun, E. Wang and J. Wang, *Chin. Sci. Bull.*, 2014, **59**, 4946–4952.
9 L. Y. Feng, Z. J. Zhang, J. S. Ren and X. G. Qu, *Biosens. Bioelectron.*, 2014, **62**, 52–58.
10 Y. He, Z. G. Wang, H. W. Tang and D. W. Pang, *Biosens. Bioelectron.*, 2011, **29**, 76–81.
11 X. Zuo, Y. Xiao and K. W. Plaxco, *J. Am. Chem. Soc.*, 2009, **131**, 6944–6945.
12 Y. Eguchi, S. Shimizu and Y. Tsujimoto, *Cancer Res.*, 1997, **57**, 1835–1840.
13 Z. Lin, F. Luo, Q. Liu, L. Chen, B. Qiu, Z. Cai and G. Chen, *Chem. Commun.*, 2011, **47**, 8064–8066.
14 J. Lu, M. Yan, L. Ge, S. Ge, S. Wang, J. Yan and J. Yu, *Biosens. Bioelectron.*, 2013, **47**, 271–277.
15 Y. Song, X. Yang, Z. Li, Y. Zhao and A. Fan, *Biosens. Bioelectron.*, 2014, **51**, 232–237.
16 Z. M. Zhou, Y. Yu and Y. D. Zhao, *Analyst*, 2012, **137**, 4262–4266.
17 Y. H. Song, X. Yang, Z. Q. Li, Y. J. Zhao and A. P. Fan, *Biosens. Bioelectron.*, 2014, **51**, 232–237.
18 R. C. Gao, C. H. Xue, L. Yuan, Z. J. Li, Y. Xue, F. Cui and Y. Sun, *J. Chromatogr. A*, 2006, **1118**, 278–280.
19 M. Kulp and M. Kaljurand, *J. Chromatogr. A*, 2004, **1032**, 305–312.
20 H. Gao, M. Xi, L. Xu and W. Sun, *Microchim. Acta*, 2011, **174**, 115–122.
21 S. Zhang, A. Bao, T. Sun, E. Wang and J. Wang, *Biosens. Bioelectron.*, 2015, **63**, 287–293.
22 J. R. Chen, X. X. Jiao, H. Q. Luo and N. B. Li, *J. Mater. Chem. B*, 2013, **1**, 861–864.
23 W. D. Pu, L. Zhang and C. Z. Huang, *Anal. Methods*, 2012, **4**, 1662–1666.
24 L. Zhang, H. Wei, J. Li, T. Li, D. Li, Y. Li and E. Wang, *Biosens. Bioelectron.*, 2010, **25**, 1897–1901.
25 F. Li, Z. F. Du, L. M. Yang and B. Tang, *Biosens. Bioelectron.*, 2013, **41**, 907–910.
26 Y. Wang, L. Bao, Z. Liu and D. W. Pang, *Anal. Chem.*, 2011, **83**, 8130–8137.
27 S. Zhang, K. Wang, Z. Li, Z. Feng and T. Sun, *RSC Adv.*, 2015, **5**, 44714–44721.
28 L. N. Zhang, H. H. Deng, F. L. Lin, X. W. Xu, S. H. Weng, A. L. Liu, X. H. Lin, X. H. Xia and W. Chen, *Anal. Chem.*, 2014, **86**, 2711–2718.
29 S. P. Li, L. Q. Wang, Y. Q. Hao, L. L. Zhang, B. B. Zhou, L. Deng and Y. N. Liu, *RSC Adv.*, 2014, **4**, 23185–23190.
30 J. J. Wang, J. X. Lu, S. Su, J. M. Gao, Q. Huang, L. H. Wang, W. Huang and X. L. Zuo, *Biosens. Bioelectron.*, 2015, **65**, 171–175.
31 S. Cheng, B. Zheng, M. Z. Wang, M. H. W. Lam and X. W. Ge, *Talanta*, 2013, **115**, 506–511.
32 J. Wang, L. Wang, X. Liu, Z. Liang, S. Song, W. Li, G. Li and C. Fan, *Adv. Mater.*, 2007, **19**, 3943–3946.
33 V. Guieu, C. Ravelet, S. Perrier, Z. Y. Zhu, S. Cayez and E. Peyrin, *Anal. Chim. Acta*, 2011, **706**, 349–353.
34 X. Y. Lin, L. Cui, Y. S. Huang, Y. Lin, Y. Xie, Z. Zhu, B. C. Yin, X. Chen and C. J. Yang, *Chem. Commun.*, 2014, **50**, 7646–7648.
35 M. Il Kim, M. S. Kim, M. A. Woo, Y. Ye, K. S. Kang, J. Lee and H. G. Park, *Nanoscale*, 2014, **6**, 1529–1536.
36 C. Ray, S. Dutta, S. Sarkar, R. Sahoo, A. Roy and T. Pal, *J. Mater. Chem. B*, 2014, **2**, 6097–6105.
37 X. Q. Wu, Y. Xu, Y. L. Chen, H. Zhao, H. J. Cui, J. S. Shen and H. W. Zhang, *RSC Adv.*, 2014, **4**, 64438–64442.
38 D. E. Huizenga and J. W. Szostak, *Biochemistry*, 1995, **34**, 656–665.
39 X. Gong, J. F. Li, W. J. Zhou, Y. Xiang, R. Yuan and Y. Q. Chai, *Anal. Chim. Acta*, 2014, **828**, 80–84.
40 C. Li, M. Numata, M. Takeuchi and S. Shinkai, *Angew. Chem., Int. Ed.*, 2005, **44**, 6371–6374.
41 J. Li, H. E. Fu, L. J. Wu, A. X. Zheng, G. N. Chen and H. H. Yang, *Anal. Chem.*, 2012, **84**, 5309–5315.
42 W. J. Chen, Y. P. Hu, J. S. Li, Y. H. Li, J. H. Bai, J. Zheng and R. H. Yang, *Anal. Methods*, 2014, **6**, 3219–3222.
43 S. Ye, J. Xiao, Y. Guo and S. Zhang, *Chem.–Eur. J.*, 2013, **19**, 8111–8116.
44 L. Lu, J. C. Si, Z. F. Gao, Y. Zhang, J. L. Lei, H. Q. Luo and N. B. Li, *Biosens. Bioelectron.*, 2015, **63**, 14–20.

